Multicomponent Protein Adsorption in Supported Cationic Polyacrylamide Hydrogels

Shawn M. Russell and Giorgio Carta
Dept. of Chemical Engineering, University of Virginia, Charlottesville, VA 22904

DOI 10.1002/aic.10482
Published online June 8, 2005 in Wiley InterScience (www.interscience.wiley.com).

Partitioning and transport of proteins in charged polyacrylamide gels were studied for single and two-component protein mixtures. The gels were synthesized within fused-silica capillaries allowing a direct microscopic determination of concentration profiles in the gel during adsorption and desorption of fluorescently labeled proteins. α-lactalbumin, ovalbumin, and BSA were used as model proteins spanning molecular masses between 15 and 65 kDa. The proteins were conjugated to green and red rhodamine fluorescent labels, allowing simultaneous and independent determinations of two proteins during binary adsorption. The proteins were found to be favorably but reversibly partitioned into the gel and could be eluted at high salt concentrations. The transient concentration profiles were found to be consistent with a Fickian diffusion model with a driving force based on the adsorbed phase concentration gradient. The diffusivity and adsorption capacity of the proteins determined from the microscopic data compared favorably to results previously obtained from macroscopic studies of Q-HyperD, a gel-filled particle chemically similar to the gels synthesized in this work. Coadsorption and sequential adsorption experiments also resulted in diffuse concentration profiles indicating that the underlying transport mechanism is the same as for single component transport. The diffusion model was extended to predict the two-component cases. Predictions were reasonably accurate for co-adsorption, but gave rates higher than seen experimentally for sequential adsorption, probably as a result of diffusion flux coupling or other nonidealities. © 2005 American Institute of Chemical Engineers *AIChE J,* 51: 2469–2480, 2005
Keywords: diffusion, proteins, charged polymer gels, ion exchange

Introduction

Charged gels are of interest for ion-exchange chromatographic separation of proteins,[1-2] as well as for biomedical applications for drug delivery, and as components in diagnostic devices.[3-4] Although freestanding hydrogels are not ideal for chromatographic separations due to their modest mechanical strength and osmotic stability,[5-6] composite materials incorporating a gel within the pores of rigid particles or membranes have been shown to be stable against mechanical and osmotic forces making these gels useful for practical applications.[6-8]

Correspondence concerning this article should be addressed G. Carta at gc@virginia.edu.

Two important considerations in the application of these materials to protein chromatography are partitioning and transport. Unlike neutral gels, partitioning of oppositely charged macromolecules in charged gels can be very favorable.[9] As a result, proteins can be highly concentrated. Transport rates are often limiting. However, while the diffusivity of macromolecules in these gels is lower than in free solution, high mass-transfer rates can be obtained because of the large diffusional driving force.[10]

A number of macroscopic studies on protein adsorption on commercially available gel-composite media known as HyperD have been conducted.[11-16] These materials consist of porous silica or ceramic particles filled with a charged polyacrylamide hydrogel. They have been shown to possess a high protein binding capacity and high mass-transfer rates, which

exceed the rates predicted for diffusion in the liquid phase. Phenomenological models accounting for a diffusive flux within the adsorbed phase have been employed for these materials.[13-15] However, only limited insight can be obtained by modeling the results of macroscopic studies since different rate models often yield qualitatively similar uptake curves.[17-18] As a result, it is difficult to ascertain the transport mechanism. On the other hand, microscopic measurements of concentration profiles provide greater insight in this regard since different mass-transfer mechanisms are expected to result in qualitatively different profiles during transient adsorption and desorption. Confocal microscopy has been used for this purpose by a number of authors to study protein transport in particles.[19-23] Transport in charged gels synthesized within small capillaries can also be observed directly by ordinary microscopic methods as shown by Lewus and Carta.[24-25] Compared to measurements with spherical particles, the linear geometry of the capillaries provides the advantage of a simpler quantitative analysis and overcomes fluorescence attenuation effects encountered with confocal microscopy. Moreover, using capillaries of sufficient length, the physical situation approximates a semiinfinite slab geometry, which allows a simple calculation of the diffusivity.

In previous work, Lewus and Carta studied the partitioning and transport of cytochrome *c* (a positively charged protein at the experimental conditions) within an anionic acrylamide-based hydrogel.[24] Russell et al. extended this work to the corresponding cationic gel using negatively charged myoglobin.[10] Both of these proteins are colored and were observed with visible light microscopy. As a result, only single component adsorption experiments could be carried out. Since multicomponent transport is of both practical and fundamental interest, we now extend this work further to binary protein mixtures. Proteins conjugated to fluorescent labels are used to determine concentration profiles in capillary supported gels by epifluorescent microscopy. Adsorption isotherms and transport properties are first determined for three individual proteins with molecular mass between 15,000 and 65,000. Measurements are then conducted for co-adsorption and sequential adsorption of protein mixtures. Finally, a phenomenological diffusion model is used for a quantitative analysis of the single component results and for a prediction of binary adsorption.

Materials and Methods

Preparation of Gels

Optically clear, cationic gels were synthesized within the lumen of fused silica capillaries having a square section as described by Russell et al.[10] As in our previous work, 1-cm long sections of capillaries with 100 and 300 μm inside and outside dimensions (Polymicro Technologies, Phoenix, AZ) were stripped of their polymer coating and treated with bind-silane (γ-methacryloxy-propyl-trimethoxysilane from Amersham Pharmacia Biotech, Piscataway, NJ). The treated capillaries were then filled with a solution containing a water-soluble functionalized monomer (3-methacryloylamino)propyl trimethyl ammonium chloride - MAPTAC), a crosslinker (N,N' methylene bis-acrylamide - MBA), an initiator (ammonium persulfate - AP), and a promoter (N,N,N',N - tetramethyl ethylenediamine - TEMED). These chemicals were obtained from Sigma Chemical Co. (St. Louis, MO), and were used in the proportion of 0.15 g MAPTAC, 0.0075 g MBA, 0.0075 g AP, and 1 μL TEMED per cm^3 of solution prepared with distilled, deionized, degassed water. Polymerization occurs rapidly after mixing and loading into the capillaries and is complete in less than an hour. Following polymerization, the gel-filled capillary sections were placed in a 50 mol/m^3, pH 8.6 Tris-HCl buffer for a minimum of 24 h. The supported cationic gel synthesized in this manner has a polymer concentration of 0.16 g/cm^3, a crosslink density of 5% (w/w), and a charge density of 682 $\mu mol/cm^3$. Because of its covalent attachment to the capillary wall via the bind-silane, the capillary-supported gel resists osmotic forces and is mechanically stable.

Protein Labeling

Bovine serum albumin (M_r~65,000, pI~4.9), ovalbumin (M_r~45,000, pI~4.6), and α-lactalbumin (M_r~15,000, pI~5.0) from Sigma Chemical Co. (St. Louis, MO) were used in this work. The proteins were labeled with fluorescent dyes following the manufacturer recommended procedures. A Beckman Coulter DU640 spectrophotometer (Fullerton, CA) was used to determine protein concentration and degree of labeling. HPLC analyses of labeled and unlabeled proteins were carried out with a 0.5 $\times$ 5 cm Source Q 15 column (Amersham Pharmacia Biosciences, Picataway, NJ). The analyses were performed with a Waters system (Milford, MA) using a 50 mol/m^3 Tris-HCl buffer at pH 8.6 as the mobile phase at a flow rate of 0.8 cm^3/min with a 0-400 mol/m^3 NaCl gradient over 20 min. Initially, ovalbumin was labeled with Alexa 488 from Molecular Probes (Eugene, OR), following prior work by Linden et al.[17] However, this label proved unsatisfactory for our system. Figure 1a shows the HPLC analyses of unlabeled ovalbumin, monitored at 280 nm, and the Alexa-ovalbumin conjugate, monitored at both 280 and 494 nm. The latter is the absorbance maximum of the Alexa molecule. Obviously, there is a large difference in retention time between labeled and unlabeled protein. This shift in retention is likely due to the additional negative charges brought about by Alexa 488 (see Figure 1a). Since the Source Q functionality is the same as that of the polyacrylamide gel used in this work, it is likely that Alexa 488 would also be preferentially adsorbed on our gel, which could produce artifacts in the measurements. We, thus, turned our attention to rhodamine dyes. These dyes have no net charge (see Figure 1b and c) and are available with noninterfering excitation and emission spectra. Rhodamine green (RG, excitation maximum at 505 nm, emission maximum at 527 nm) and tetramethylrhodamine isothiocyanate (TRITC, excitation maximum at 555 nm, emission maximum at 580 nm) from Molecular Probes were used in our work. We also obtained a TRITC-BSA conjugate directly from Sigma. Conjugation was done by reacting a 10 mg/cm^3 protein solution with 1 mg/cm^3 of the label dissolved in DMSO for 1 h. The reaction mixture was then separated in a 10 cm column filled with Sephadex G25 particles. HPLC analyses of the RG and TRITC conjugates are shown in Figure 1b and c. It can be seen that the shift in retention time between labeled and unlabeled protein, summarized in Table 1, is very small suggesting that the rhodamine protein conjugates behave in a manner similar to the corresponding native protein. In contrast, the difference between the Alexa-ovalbumin conjugate and ovalbumin is as large as the difference between ovalbumin and BSA indicating that this

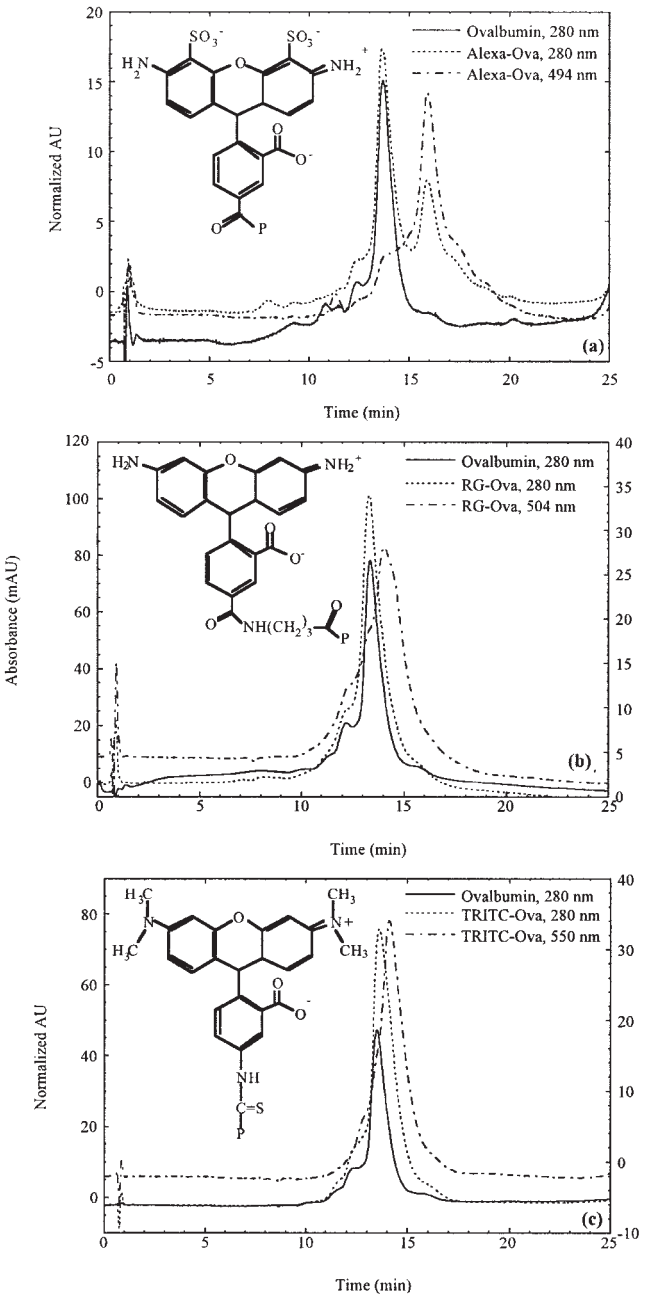

Figure 1. Anion exchange HPLC analyses of labeled and unlabeled ovalbumin.

Insets show structures of fluorescent labels with P indicating the protein attachment site. Analysis conditions are noted in the text. (a) Alexa 488, (b) Rhodamine Green (RG), and (c) Tetramethyl Rhodamine Isothiocyanate (TRITC).

label would be completely inadequate for multicomponent studies.

Apparatus for transient mass-transfer studies

The apparatus used to determine the concentration profiles in the capillary-supported gels is the same as that described by Russell et al.[10] It comprises a flow cell consisting of a 1/8-in thick Teflon slab sandwiched between two microscope slides. Silicon gaskets were placed between the glass slides, and the Teflon slab and two aluminum plates were used to hold the flow system together. Side ports on the short sides of the Teflon slab were used for flow of the protein solutions. The gel-filled capillaries were mounted on syringe tips with a cyanoacrylate adhesive and inserted in a hole through the side of the Teflon slab with the open end of the capillary projecting in the center of the fluid flow path. Identical capillaries filled with protein solutions and sealed at both ends with the cyanoacrylate adhesive were also inserted through a second hole in the Teflon slab and used as calibration standards. Protein solutions containing 0.25% (w/w) of labeled protein were prepared in a 50 mol/m^3 Tris-HCl buffer at pH 8.6. At this pH, our proteins have a strong negative charge and are favorably partitioned into our positively charged gel. Protein solutions were fed to the flow cell with a Cole-Parmer (Chicago, IL) peristaltic pump at a flow rate of 0.7 cm^3/min. The latter corresponds to a velocity past the exposed tip of the capillary of about 185 cm/h. All experiments were performed at room-temperature (20 $\pm$ 2°C).

A Nikon Eclipse E200 epifluorescence microscope with a high-pressure mercury lamp was used at 100x magnification. Nikon B-2A (EX 450-490 nm, DM 500 nm, EM 520-550) and G2-E/C (EX 528-553 nm, DM 565 nm, BA 600-660 nm) filter sets were used for the independent acquisition of fluorescence emissions from RG and TRITC labeled proteins. The emission component of the B-2A filter was obtained from Chroma Technology Corp (Brattleboro, VT). Digital images were obtained with a Sanyo Hi-Resolution Color CCD camera interfaced to a Power Mac 7100/80 computer. NIH Image (a public domain program developed at the U.S. National Institute of Health and available on the Internet at http://rsb.info.nih.gov/nih-image/), was used for image analysis. A linear calibration curve relating the protein concentration to the signal intensity was generated with the calibration capillaries, and used to convert the raw fluorescence data for adsorption in the capillary supported gels to adsorbed protein concentrations. Two component calibrations showed minimal interference between the RG and TRITC channels.

Results and Discussion

Equilibrium studies

The equilibrium adsorption capacity of the gel was obtained by placing gel-filled capillaries in different protein solutions for a minimum of 72 h. The capillaries used for these determinations were about 0.5 cm in length and exposed to the protein solutions at both ends. The capillaries were removed from solution and placed under the microscope to determine the

Table 1. Retention Times of Native Protein and Labeled Proteins in High Resolution Gradient Elution Anion Exchange Chromatography with Source 15 Q

	Retention Time (min)			
Protein	Unlabeled	Alexa 488 Conjugate	TRITC Conjugate	RG Conjugate
α-Lactalbumin	10.1			10.5
Ovalbumin	13.4	16.0	14.0	14.0
BSA	16.1		16.3	

Gradient: 0–400 mol/m^3 NaCl in 20 min.
Other conditions are given in text.

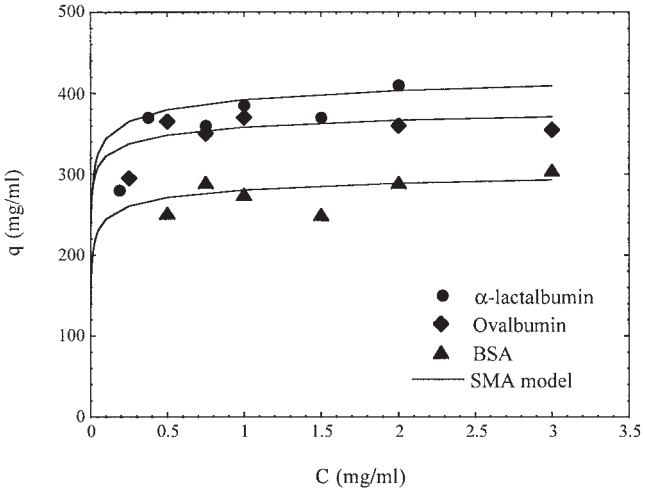

Figure 2. Single component adsorption isotherms in 50 mol/m^3 TrisHCl buffer at pH 8.5.

Lines are calculated from SMA model with parameters in Table 2.

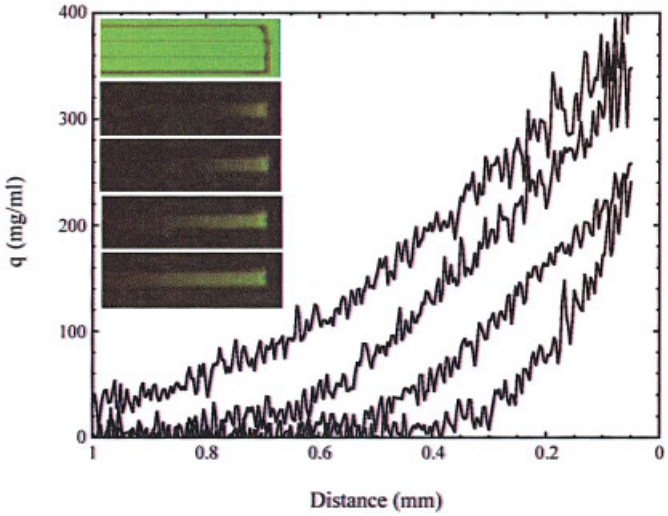

Figure 3. Adsorption of 1 mg/cm^3 ovalbumin with RG-ovalbumin tracer. Profiles and digital images are shown at 1, 2, 4, and 8 h.

The top image shows a visible image of the capillary supported gel. Approximately 1 mm of the capillary is visible.

adsorbed protein concentration from the fluorescence signals. Since the capillaries were not completely saturated even after 72 h, the adsorbed protein concentration was determined near the exposed ends, where equilibrium was attained. This was demonstrated by the fact that values obtained in this manner at 24 h did not differ significantly from the values determined at 72 h. Adsorption isotherms are shown in Figure 2. Partitioning is obviously quite favorable for all three proteins with capacities between 300 and 400 mg/cm^3 of gel. In a previous study, Fernandez and Carta have reported the equilibrium binding capacities for the same three proteins on Q-HyperD to be between 220 and 240 mg/cm^3 for the same low ionic strength.[13] As previously discussed, the Q-HyperD media consists of a polyacrylamide gel similar to that used in this work but contained within the pores of silica particles. Since the porosity of the Q-HyperD silica support matrix is about 0.6 and only the gel contributes to protein retention, the capacities determined by Fernandez ands Carta correspond to values between 370 and 400 mg/cm^3 when expressed on a gel-volume basis. These values are in excellent agreement with the capacities obtained for our capillary-supported gels.

Single component results

The evolution of concentration profiles in the gel during adsorption of α-lactalbumin, ovalbumin, and BSA is shown in Figures 3–5. The plots give the scaled concentration profiles at different times along with the corresponding digital images. (Images are reproduced in black and white, but original color images can be viewed in the online version). Because of imperfections at the tip of the capillary, the profiles could not be extended reliably to the very edge of the gel. Nonetheless, the trends are clear. The adsorbed protein concentration at the tip of the gel quickly arrives at a constant value while diffuse profiles are established through the gel. The profiles evolve in time while retaining a diffuse character. This result is consistent with previous observations by Lewus and Carta and Russell et al. and suggests that these proteins retain diffusional mobility in the gel.[10, 25] If this were not the case, much sharper profiles would be expected, as a result of the extremely favorable nature of the equilibrium isotherms.

The effect of protein concentration in solution is shown in Figure 6 for all three proteins. As an example, the images in this figure show ovalbumin adsorption in the gel at 1 h and 4 h for experiments with 1 and 2 mg/cm^3 solution concentrations. The background fluorescence intensity was obviously larger for the 2 mg/cm^3 experiment since the ratio of labeled and unlabeled protein was kept constant. The fluorescence intensity in the gel also appears to be greater for the 2 mg/cm^3 experiment. However, this was due to variations of the intensity of the light source. In fact, when the fluorescence intensity was normalized by subtracting the solution background and multiplied times

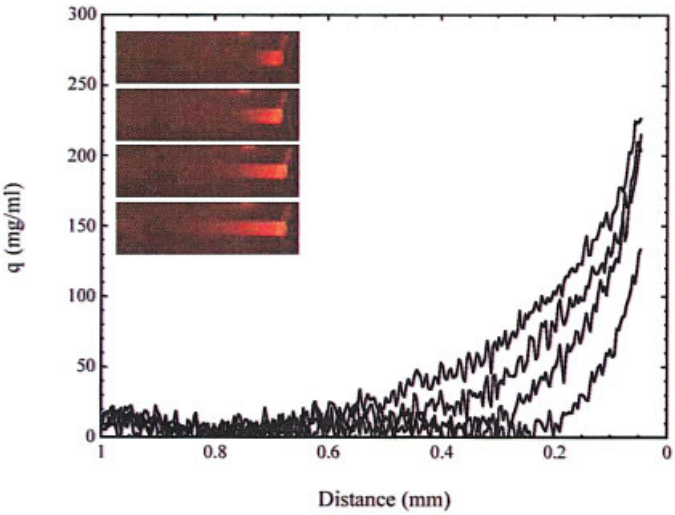

Figure 4. Adsorption of 1 mg/cm^3 BSA with TRITC-BSA tracer. Profiles and digital images are shown at 1, 2, 4, and 8 h.

the appropriate calibration constant, the adsorbed concentration and depths of penetration were found to be essentially the same at the two different solution concentrations. This can be seen more clearly from the digitized, scaled profiles shown in this figure, which are nearly coincident. Since the solution concentrations used in these experiments lie in the flat portion of the isotherm (cf. Figure 2), coincident profiles signify that protein transport is dependent on an adsorbed phase driving force. As a result, nearly identical transport rates are obtained at the two different solution concentrations.

The reversibility of adsorption of labeled protein and diffusional mobility in these gels is demonstrated further in Figure 7 using TRITC-ovalbumin as a tracer. In this experiment, the gel was exposed to unlabeled ovalbumin for a 3 h period, to ovalbumin containing 0.25% TRITC-ovalbumin for the next 3 h, and again to unlabeled ovalbumin alone for the rest of the experiment. As seen in this figure, TRITC-ovalbumin diffuses in the partially ovalbumin loaded gel. The rate is slower than for the initial adsorption in a clean gel (cf. Figure 3), but this is expected since an established ovalbumin concentration profile already existed when the gel was first exposed to TRITC-ovalbumin. Following removal of TRITC-ovalbumin from solution, desorption of this tracer from the gel ensues. It can be seen that while desorption occurs at the exposed end of the capillary, a fraction of the TRITC-ovalbumin continues to diffuse toward the unexposed end. In summary, TRITC-ovalbumin appears to behave as a tracer that is essentially undifferentiated from the unlabeled protein. Because diffusional mobility is apparently preserved in these gels, reversible adsorption and desorption of the tracer is seen in response to concentration changes in solution. Although not shown here, similar results were obtained for TRITC-BSA and BSA solutions in an analogous experiment. The rates were, however, lower, consistent with the previous adsorption results.

An additional single component result is shown in Figure 8 for desorption of ovalbumin with 500 mol/m^3 NaCl in 50 mol/m^3 TRIS buffer after exposing the gel to 1 mg/cm^3 ovalbumin for 4 h. It can be seen that the salt quickly displaces the protein. At the tip, the protein concentration approaches zero rapidly and the displaced protein exits the gel. Approximately 90% of the protein is desorbed in 2 h. Rapid diffusion of the protein out of the gel for these conditions is likely due to electrostatic shielding of the charges in the gel by the high salt concentration which overcomes the high affinity of the negatively charged protein for the positively charged gel.

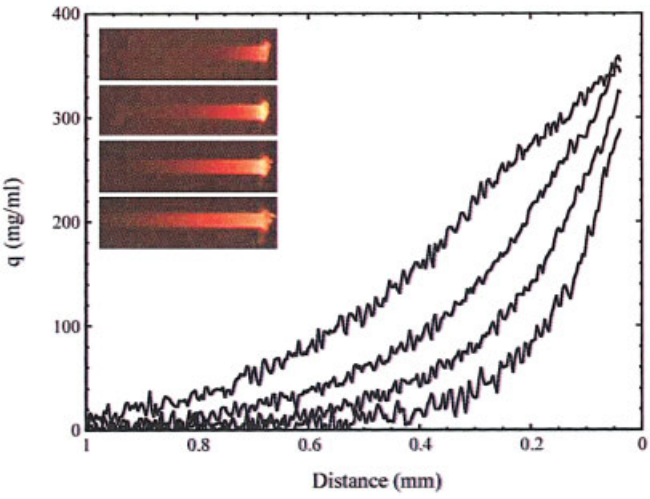

Figure 5. Adsorption of 1 mg/cm^3 α-lactalbumin with TRITC-lactalbumin tracer. Profiles and digital images are shown at 1, 2, 4, and 8 h.

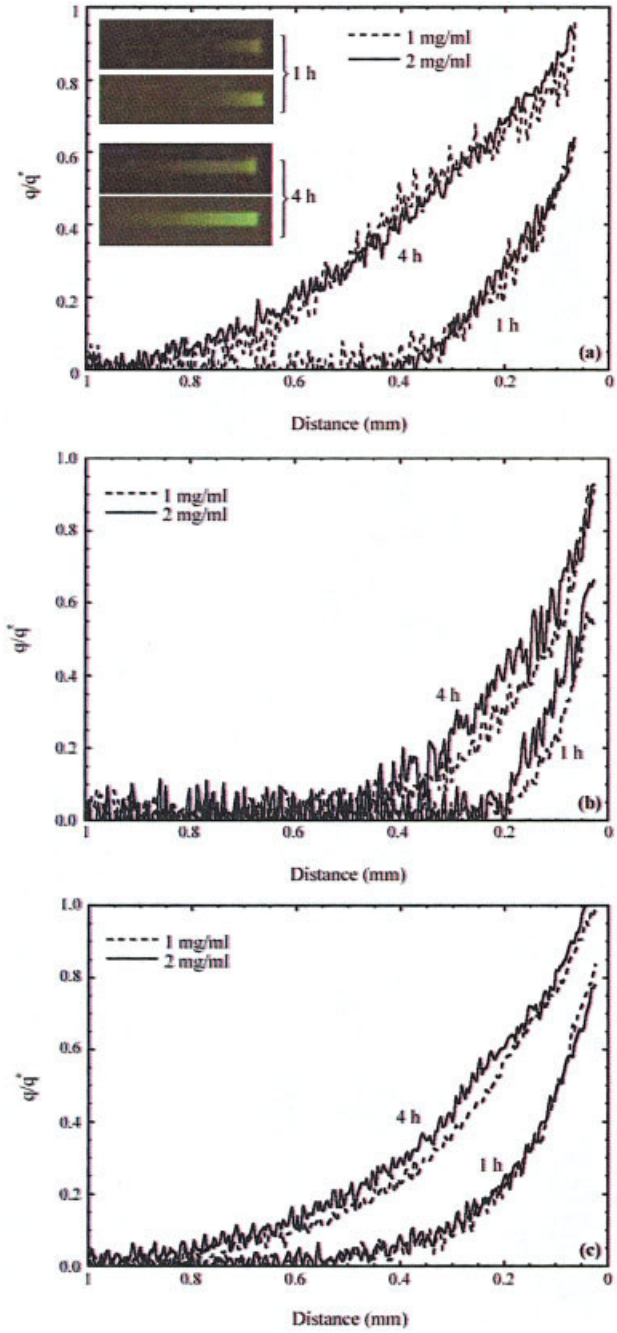

Figure 6. Adsorption of ovalbumin (a), BSA (b), and α-lactalbumin (c) at 1 and 2 mg/cm^3 solution concentrations.

Profiles are shown at 1 and 4 h. Digital images for ovalbumin in the top panel inset are for 1 mg/cm^3 (top) and 2 mg/cm^3 (bottom) solution concentrations.

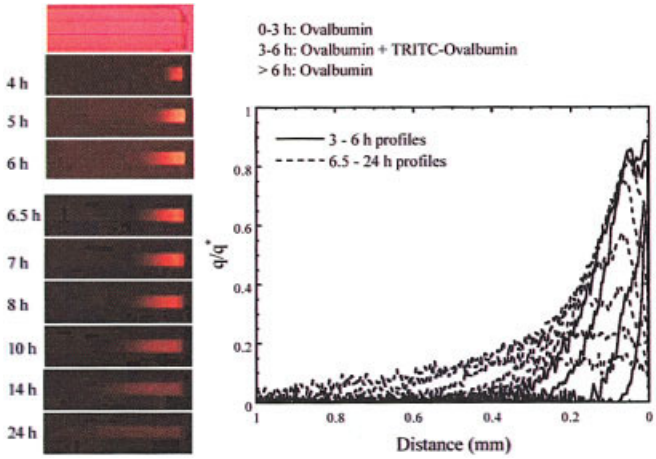

Figure 7. Adsorption of 1 mg/cm^3 ovalbumin with TRITC-ovalbumin tracer.

The gel was exposed to unlabeled ovalbumin for 3 h, to ovalbumin containing 0.25% TRITC-ovalbumin for the next 3 h, and to unlabeled ovalbumin for the remaining time. Profiles and digital images are shown at 4, 5, 6, 6.5, 7, 8, 10, 14, and 24 h. The top image shows a visible image of the capillary supported gel.

Multicomponent results

Two component coadsorption and sequential adsorption experiments were conducted for mixtures of ovalbumin and BSA and for mixtures of α-lactalbumin and ovalbumin using TRITC and RG conjugates as tracers. Coadsorption results are shown in Figures 9 and 10. In both cases, neither protein adsorbs so strongly that the other is excluded. As a result the proteins competitively partition and diffuse in the gel. The concentration profiles are analogous to the single component case, but with lower adsorbed concentrations for each protein. Although not shown, similar co-adsorption experiments were also run

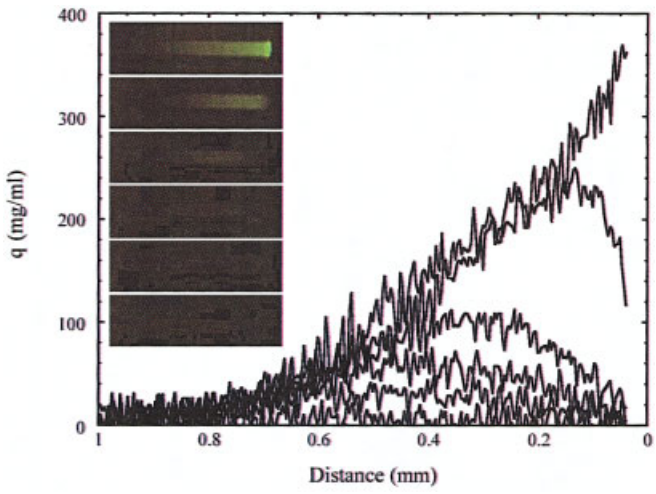

Figure 8. Desorption of ovalbumin with RG-ovalbumin tracer in 500 mol/m^3 NaCl. The gel was initially exposed to 1 mg/cm^3 ovalbumin/RG-ovalbumin in 50 mol/m^3 Tris buffer for 4 h.

Profiles and digital images are shown at 4, 4.1, 4.5, 5, 6, and 10.5 h.

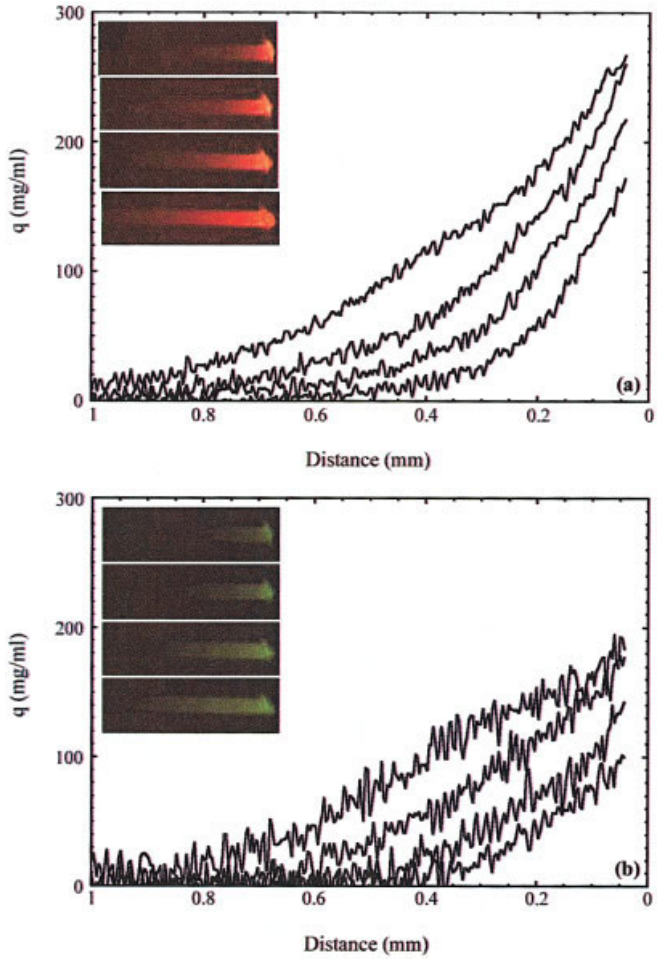

Figure 9. Coadsorption of 1 mg/cm^3 α-lactalbumin (a), and ovalbumin (b), with TRITC-lactalbumin and RG-ovalbumin tracers.

Profiles and digital images are shown at 1, 2, 4, and 8 h.

with different protein solution concentration ratios (1 to 3 and 3 to 1). The profiles were qualitatively similar to those in Figures 9 and 10, but with lower adsorbed concentrations for the protein present in lower solution concentration.

Sequential adsorption results are shown in Figures 11 and 12 for ovalbumin followed by α-lactalbumin and for the reverse, respectively. In both cases, RG-lactalbumin and TRITC-ovalbumin were used as tracers. Digital images of green and red fluorescence are shown starting at the time of the protein switch along with the digitized, scaled profiles. As seen in Figure 11, α-lactalbumin gradually displaces ovalbumin at the interface and diffuses in the gel. Ovalbumin continues to diffuse into the gel ahead of the α-lactalbumin profile, although a distinct region of the gel exists where both proteins are present in comparable concentrations. As seen in Figure 12, similar trends are observed when the gel was exposed to the two proteins in reverse order. In this case, however, the timescale for desorption of α-lactalbumin is longer, probably because this protein partitions more favorably into the gel compared to ovalbumin. Similar results (not shown) were obtained for the sequential adsorption of ovalbumin and BSA, although here

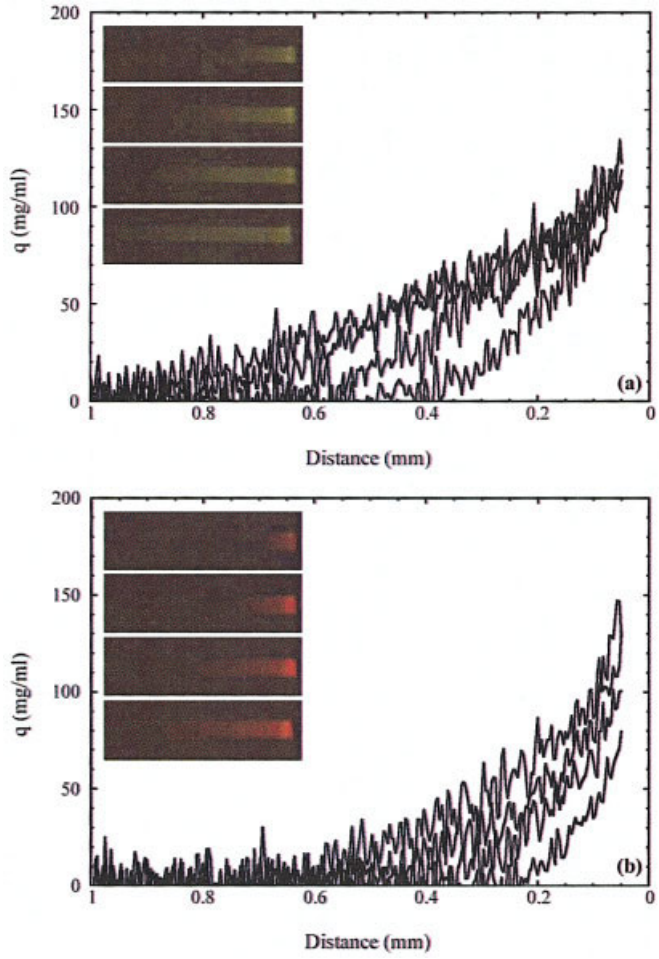

Figure 10. Coadsorption of 1 mg/cm^3 ovalbumin (a), and BSA (b), with RG-ovalbumin and TRITC-BSA tracers.

Profiles and digital images are shown at 1, 2, 4, and 8 h.

much longer timescales were required owing to the smaller diffusivity of BSA.

Mass-Transfer Modeling

Modeling mass transfer in our system requires a description of equilibrium at the gel-fluid interface, as well as a model to describe diffusional transport within the gel. A quantitative analysis is conducted first for the single component case and then extended in an approximate way to binary adsorption.

Single component analysis

Following Fernandez and Carta,[13] a description of the adsorption isotherms can be obtained with the Steric Mass Action (SMA) model of Brooks and Cramer[26] given by

$$C_i = \frac{q_i C_I^{z_i}}{K_i[q_o - (z_i + \sigma_i)q_i]^z} \tag{1}$$

where C_i and C_I are the protein and counterion solution concentrations, q_i is the adsorbed phase protein concentration, z_i is the protein effective charge, K_i is the equilibrium constant, and σ_i is the steric hindrance parameter. The parameters determined by data fitting for each protein are given in Table 2, and calculated lines are shown in Figure 2. The z-values are similar to those determined for these proteins in Q-HyperD and for other proteins with similar molecular masses in various ion exchange media.[13,27-28] The σ-values increase with molecular mass, which is also consistent with previous observations.[28-30]

Modeling transport in the gel is based on a phenomenological description expressed by the following equations and boundary conditions

$$\frac{\partial q_i}{dt} = \frac{\partial}{\partial z}\left[D_{s,i}(q_i)\frac{\partial q_i}{\partial z}\right] \tag{2}$$

$$t = 0, \quad q = 0 \tag{2a}$$

$$z = 0, \quad -D_{s,i}\frac{\partial q_i}{\partial z} = k_f(C_i - C_i^*) \tag{2b}$$

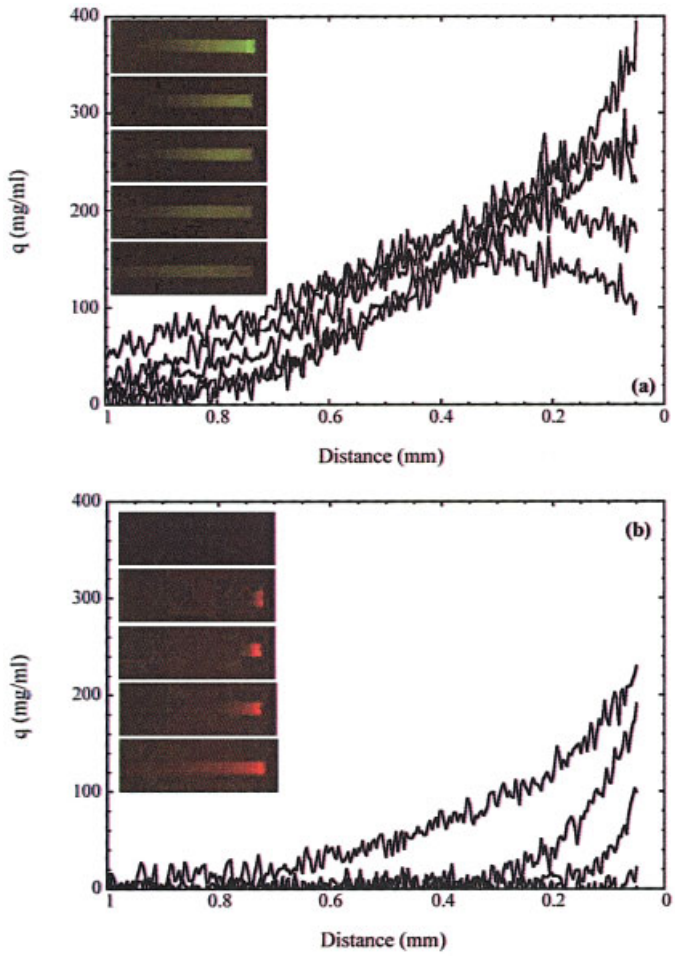

Figure 11. Sequential adsorption of 1 mg/cm^3 ovalbumin followed by 1 mg/cm^3 α-lactalbumin.

Profiles and digitized images are shown at 4, 5, 6, 8, and 14 h. (a) ovalbumin, (b) α-lactalbumin.

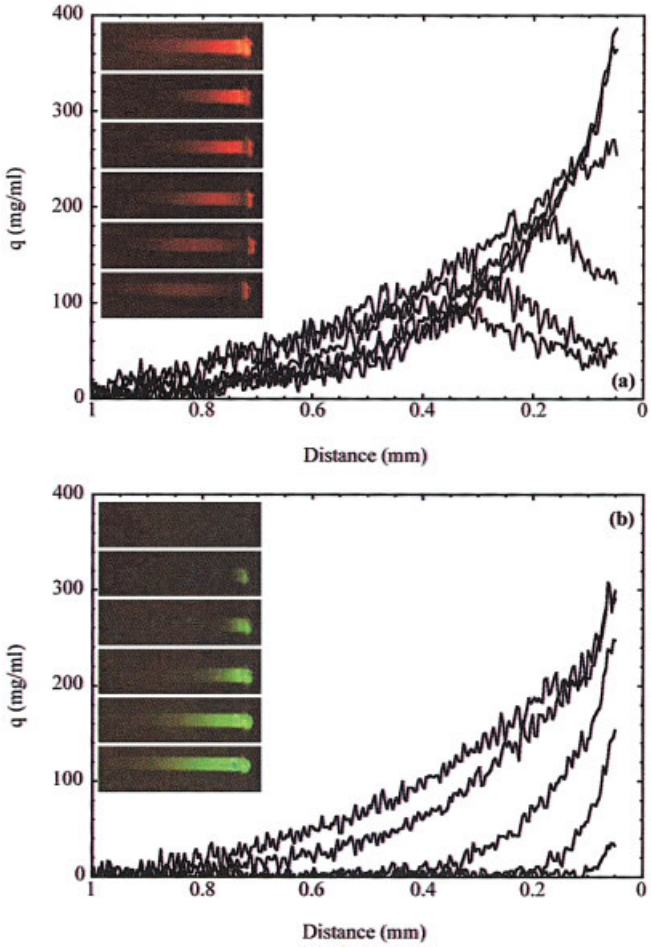

Figure 12. Sequential adsorption of 1 mg/cm^3 α-lactalbumin followed by 1 mg/cm^3 ovalbumin.

Profiles and digitized images are shown at 4, 5, 6, 8, 12, and 24 h. (a) α-lactalbumin, (b) ovalbumin.

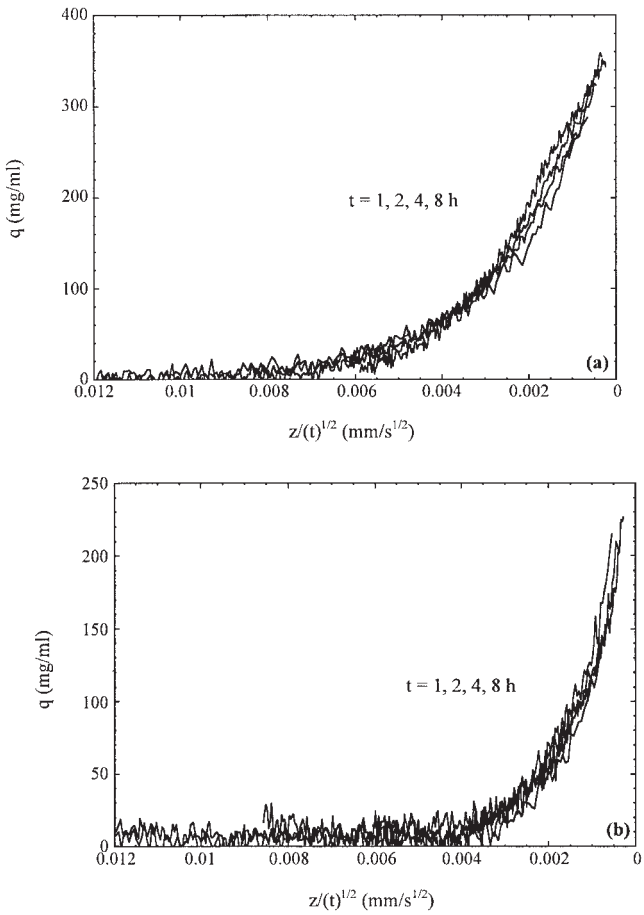

Figure 13. Concentration profiles for single component adsorption 1 mg/cm^3 BSA (a) and α-lactalbumin (b) plotted according to Boltzmann transformation.

Profiles at 1, 2, 4, and 8 h. Data are from Figure 4 and 5.

$$z \rightarrow \infty, \quad \frac{\partial q_i}{\partial z} = 0 \tag{2c}$$

where $D_{s,i}$ is the protein diffusivity in the gel, k_f is the boundary layer mass transfer coefficient, and C_i and C_i^* are the bulk and interfacial solution concentrations, respectively. If k_f is neglected, an assumption valid for long times, consistency of the experimental concentration profiles with this general Fickian diffusion model can be demonstrated by replotting the profiles according to the Boltzmann transformation variable $\eta = z/\sqrt{t}$. Examples are shown in Figure 13 for BSA and α-lactalbumin. The self-similarity of the profiles according to the Boltzmann transformation confirms the consistency with Eq. 2.

As shown previously,[10,25] the concentration dependent diffusivity in the gel, $D_{s,i}(q_i)$, can be obtained from an integral and a derivative of the concentration profiles. However, as shown below, a simpler formulation based on Eq. 2 with a constant diffusivity can also be used to describe the single component results. A comparison of calculated and experimental profiles is shown in Figure 14. For these calculations, we used a value of $k_f = 1 \times 10^{-3}$ cm/s, based on previous work,[25] and the experimental average values of $D_{s,i}$ for each protein. The conservation equation was solved numerically using the SMA model to describe equilibrium at the gel-fluid interface. As seen in this Figure 14, the agreement between experimental and calculated curves is quite reasonable. The average diffusivity values are summarized in Table 3 in comparison with values determined previously by Fernandez and Carta from macroscopic batch uptake experiments with Q-HyperD particles[13]. The Q-HyperD values were corrected assuming a tortuousity factor of 2 for the silica support matrix that contains the gel. Although not identical, the diffusivity values determined in this work are consistent with those for Q-HyperD particles indicating that our experimental results with capillary supported gels can be extended to a prediction of mass transfer in these chromatography matrices.

Table 2. Fitted Equilibrium Parameters

Protein	K	z	σ
α-Lactalbumin	4.0	5.0	16
Ovalbumin	1.0	6.2	63
BSA	5.0	4.6	120

Multicomponent analysis

The extension of the SMA model to binary adsorption yields the following Eqs[26]

$$q_i = K_i\left(\frac{q_I}{C_I}\right)^{z_i} C_i \tag{3}$$

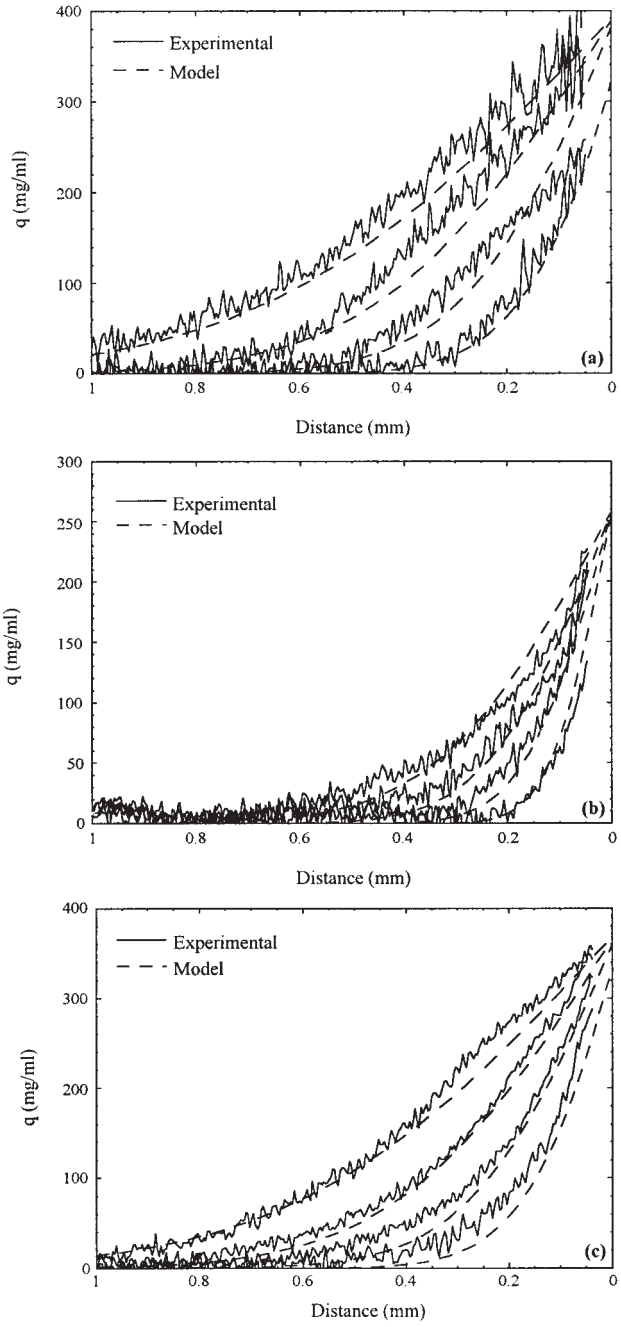

Figure 14. Experimental and calculated profiles for single component adsorption with constant diffusivity model.

(a) ovalbumin, (b) BSA, (c) α-lactalbumin. Data are from Figures 3 – 5.

Table 3. Average Diffusivities Obtained for Capillary-Supported Gels and Q-HyperD Particles

Protein	$D_{s,i}$ (cm^2/s)	$D_{s,i}$ [*Q-HyperD*] (cm^2/s)
α-Lactalbumin	4.2×10^{-8}	3.2×10^{-8}
Ovalbumin	5.0×10^{-8}	3.0×10^{-8}
BSA	1.2×10^{-8}	1.8×10^{-8}

Values for Q-HyperD obtained by Fernandez and Carta (1996) are corrected with a tortuosity factor of 2 for the silica support matrix.

$$q_I = q_0 - \sum_{j=1}^{2} (z_j + \sigma_j)\left(\frac{q_I}{C_I}\right)^{z_j} K_j C_j \tag{4}$$

Experimental adsorption capacity values obtained from the long-term exposure of capillary supported gels to binary protein mixtures with different solution concentration ratios are shown in Table 4, in comparison with predicted values. The experimental trends are predicted correctly. For example, for equal mass concentrations, in α-lactalbumin-ovalbumin mixtures, α-lactalbumin is preferentially adsorbed. Similarly, there is a slight preference for adsorption of BSA over ovalbumin in mixtures of these two proteins. Considering the semiempirical nature of the SMA model, the agreement with the experimental trends is remarkable.

Extension of the mass-transfer model to binary adsorption is not straightforward, however. Because of the high protein concentrations in the gel and potential electrokinetic effects, diffusion fluxes are likely coupled. At present, an exact theory to describe these effects in our system is not available. Nonetheless, it is instructive to compare the experimental profiles with predictions neglecting diffusional flux coupling and assuming constant diffusivities. Although these are crude assumptions, the comparison provides a useful benchmark. Figures 16 and 17 show this comparison for the coadsorption experiments. As with the single component case, the conservation equations were solved numerically using the SMA model to describe equilibrium and the gel-fluid interface. In both cases, there are substantial deviations near the exposed edge of the gel, however the depth of penetration of the two proteins is fairly well predicted.

Predicted profiles for the case of sequential adsorption are shown in Figures 18 and 19 for mixtures of α-lactalbumin and ovalbumin in comparison with the experimental data. It can be seen that in this case more considerable differences exist. In particular, the model overpredicts the rate of adsorption of the displacing protein and the rate of desorption of the protein initially present in the gel. Similar results (not shown) were found when comparing experimental and predicted profiles for sequential ovalbumin-BSA adsorption. There are several possible reasons for these more significant differences. The first, as already mentioned, is the possibility of coupling of diffusion fluxes. Obviously, these experiments involve counter-diffusion of the two proteins, which could slow down the rates. A second possibility is the potential existence of an interfacial resistance. The model assumes that equilibrium is established instantaneously at the gel-fluid interface. However, this may not be the case for counterdiffusion situations. A third possibility is the potential existence of a kinetic resistance to the displacement of the more strongly bound protein by the more weakly bound

Table 4. Experimental and Predicted Protein Uptake Equilibria for Binary Mixtures

Solution Concentrations (mg/cm^3)	α-Lactalbumin/Ovalbumin			BSA/Ovalbumin		
		q_{exp} (mg/cm^3)	q_{pred} (mg/cm^3)		q_{exp} (mg/cm^3)	q_{pred} (mg/cm^3)
1	α-Lactalbumin	280	230	BSA	160	190
1	Ovalbumin	190	160	Ovalbumin	140	140
1	α-Lactalbumin	150	140	BSA	150	120
3	Ovalbumin	220	240	Ovalbumin	220	230
3	α-Lactalbumin	380	330	BSA	250	270
1	Ovalbumin	65	61	Ovalbumin	55	50

one. Since the proteins are simultaneously interacting with multiple functional groups in the gel, it is possible that diffusional transport occurs under nonequilibrium binding conditions within the gel causing deviations from the simple model used here. Finally, it is possible that a certain degree of irreversible binding occurs over long times. Since the sequential adsorption experiments were carried out over much longer timescale, such irreversibility could have a greater effect. Despite the quantitative disagreement, however, the model reproduces the experimental trends well, suggesting that a surprisingly simple Fickian diffusion model captures the underlying transport mechanism.

Conclusions

We have extended previous work on protein partitioning and transport in charged polyacrylamide gels to proteins with a broader range of molecular masses and to the cases of coadsorption and sequential adsorption for binary protein mixtures. The negatively charged proteins considered in this work

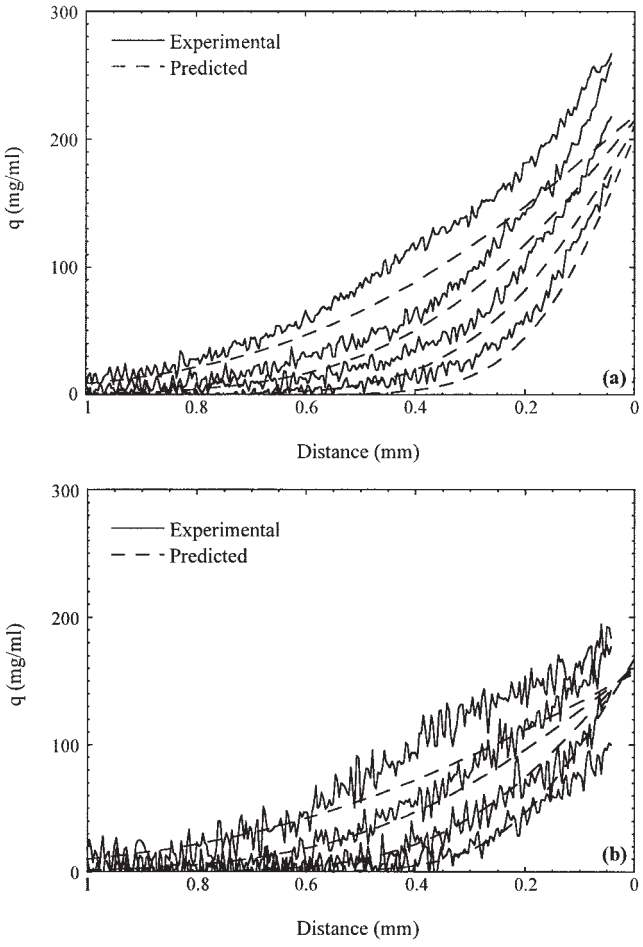

Figure 15. Experimental and predicted profiles for coadsorption of 1 mg/cm^3 α-lactalbumin and 1 mg/cm^3 ovalbumin with constant diffusivity model.

(a) α-lactalbumin, (b) ovalbumin. Data from Figure 9.

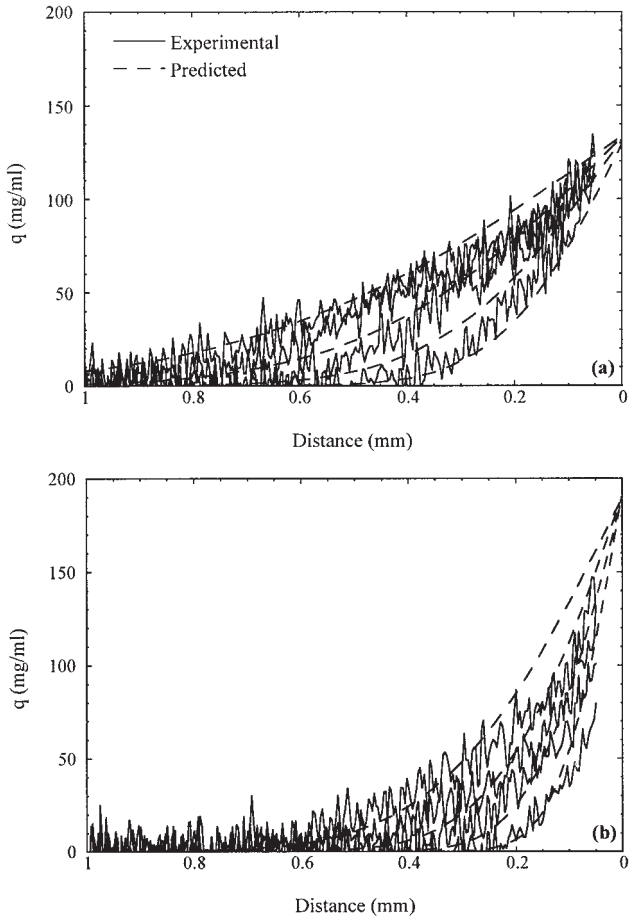

Figure 16. Experimental and predicted profiles for coadsorption of 1 mg/cm^3 ovalbumin and 1 mg/cm^3 BSA with constant diffusivity model.

(a) ovalbumin, (b) BSA. Data from Figure 10.

are very favorably, but reversibly partitioned into the gel at low ionic strength and can be desorbed completely at higher salt concentrations. The concentration profiles follow smooth broadening patterns that are self-similar and consistent with a Fickian diffusion model. Similar results are found for co-adsorption while profiles with a maximum are found for sequential adsorption in a partially saturated gel. Single component transport can be described with reasonably accuracy using a constant diffusivity. The experimental diffusivity trends merit some discussion. As was observed previously with Q-HyperD particles,[13] the diffusivities of α-lactalbumin and ovalbumin are quite similar while the diffusivity of BSA is substantially smaller. Such dramatic decline would not be expected for diffusion in open, liquid filled pores, since the hydrodynamic radii of these proteins are not vastly different. On the other hand, this behavior could be expected for transport in our homogeneous gel where the proteins diffuse in close proximity to the charged functional groups. A second observation concerns the magnitude of the diffusivity values. It should be noted that while the $D_{s,i}$-values are of the order of 10^{-8} cm^2/s, mass transfer is still quite fast because of the large driving force caused by the favorable partitioning of these proteins in the gel. A quantitative prediction of the two-component diffusion cases

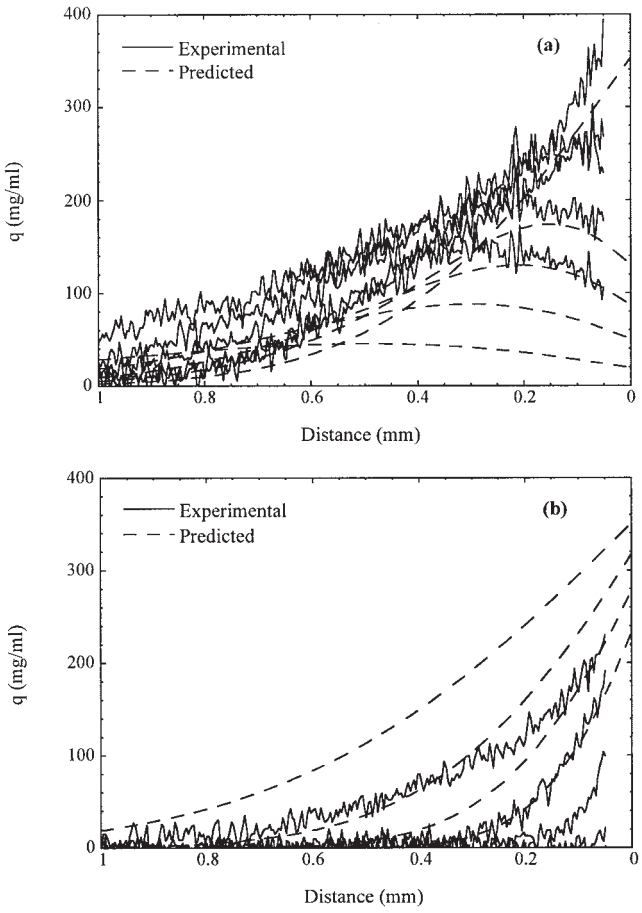

Figure 17. Experimental and predicted profiles for sequential adsorption of 1 mg/cm^3 ovalbumin followed by 1 mg/cm^3 α-lactalbumin with constant diffusivity model (data from Figure 11 (a) ovalbumin, (b) α-lactalbumin).

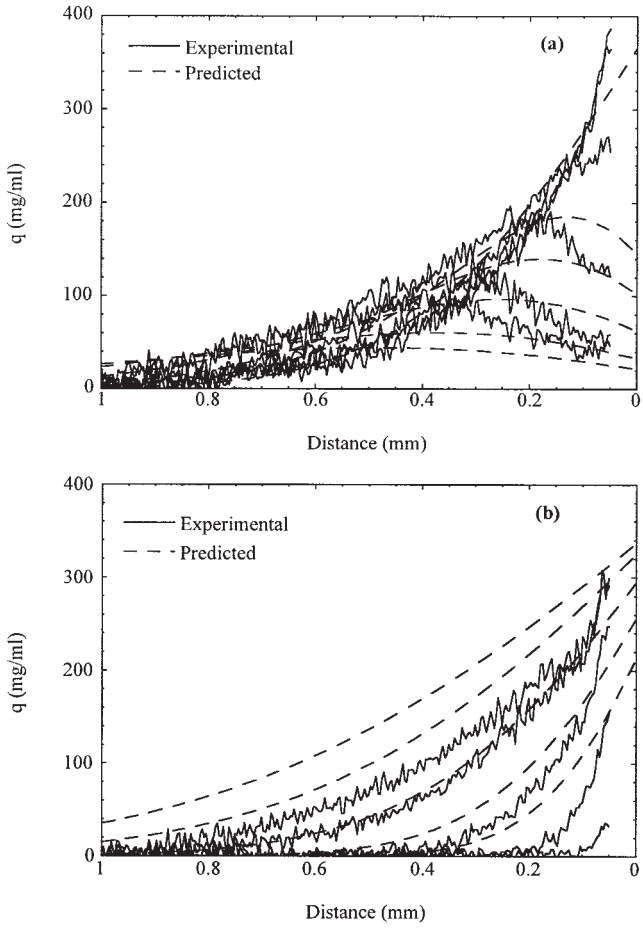

Figure 18. Experimental and predicted profiles for sequential adsorption of 1 mg/cm^3 α-lactalbumin followed by 1 mg/cm^3 ovalbumin with constant diffusivity model (data from Figure 12 (a) α-lactalbumin, (b) ovalbumin. data from Figure 12.)

was not achieved in this work. Here the situation is probably complicated by diffusional flux coupling and other nonidealities for which an exact theory is currently not available. On the other hand, a simple description using constant diffusivities is qualitatively consistent with the experimental results suggesting that the basic transport mechanism observed for single component persists in multicomponent cases.

Acknowledgment

This research was supported by NSF Grants CTS-0079334 and 0414143.

Notation

C = solution concentration, mg/cm^3
C_0 = initial solution concentration, mg/cm^3
C^* = solution concentration at gel-liquid interface, mg/cm^3
D_s = diffusion coefficient based on adsorbed-phase driving force, cm^2/s
k_f = boundary layer mass transfer coefficient, cm/s
K = SMA equilibrium constant
q = adsorbed phase concentration, mg/cm^3
q^* = equilibrium adsorbed-phase concentration, mg/cm^3
q_0 = ionic capacity, μmol/cm^3
t = time, s

z = distance into gel, cm
η = Boltzmann transformation variable, cm/s$^{1/2}$
σ = SMA hindrance parameter

Literature Cited

1. Boschetti E. Advanced sorbents for preparative protein separation purposes. *J Chromatogr. A*. 1994; 658:207-236.
2. Karlsson E, Ryden L, Brewer J. Ion-exchange chromatography. In: Janson J-C, Ryden L. Protein purification: Principles, high resolution methods, and applications. 2nd ed. New York: John Wiley & Sons, Inc., 1998:145.
3. Praveen T. Drug delivery devices. New York: Marcel Dekker, 1988.
4. Conaghey OM, Corish J, Corrigan OI. Iontophoretically assisted *in vitro* membrane transport of nicotine from a hydrogel containing ion exchange resins. *Int J Pharmaceutics*. 1998;170:215-224.
5. Baker JP, Long LH, Blanch HW, Prausnitz JM. Effect of initial total monomer concentration on the swelling behavior of cationic acrylamide-based hydrogel. *Macromolecules*. 1994;27:1446-1454.
6. Kapur V, Charkoudian JC, Kessler SB, Anderson JL. Hydrodynamic Permeability of hydrogels stabilized within porous membranes. *Ind Eng Chem Research*. 1996;35:3179-3185.
7. Girot P, Boschetti E. Passivated and stabilized porous mineral oxide supports and method for the preparation and use of the same. United States Patent No. 5,268,097. 1993.
8. Buehler KL, Anderson JL. Solvent effects on the permeability of membrane-supported gels. *Ind Eng Chem Res*. 2002;41:464-472.
9. Sassi AP, Shaw AJ, Han, SM, Blanch HW, Prausnitz JM. Partitioning of proteins and small biomolecules in temperature and pH sensitive hydrogels. *Polymer*. 1996;37:2151-2164.
10. Russell SM, Belcher EB, Carta G. Protein partitioning and transport in supported cationic acrylamide-based hydrogels. *AIChE J*. 2003;49: 1168-1177.
11. Boschetti E, Guerrier L, Girot P, Horvath J. Preparative high-performance liquid chromatographic separation of proteins with HyperD ion-exchange supports. *J Chromatogr. B*. 1995; 664:225-231.
12. Rodrigues AE, Loureiro JM, Chenou C, Rendueles de la Vega M. Bioseparations with permeable particles. *J Chromatogr. B*. 1995;664: 233-240.
13. Fernandez MA, Carta G. Characterization of protein adsorption by composite silica-polyacrylamide gel anion exchangers - I. Equilibrium and mass transfer in agitated contactors. *J Chromatogr. A*. 1996;746: 169-183.
14. Weaver LE, Carta G. Protein adsorption on cation exchangers: comparison of macroporous and gel-composite media. *Biotechnol Progr.* 1996;12:342-355.
15. Wright PR, Muzzio FJ, Glasser BJ. Batch uptake of lysozyme: effect of solution viscosity and mass transfer on adsorption. *Biotechnol Progr*. 1998; 14:913-921.
16. Lewus RK, Carta G. Binary protein adsorption on gel-composite ion-exchange media. *AIChE J*. 1999;45:512-522.
17. Linden T, Ljunglöf A, Hagel L, Kula MR, Thömmes J. Visualizing patterns of protein uptake to porous media using confocal scanning laser microscopy. *Sep Sci Technol.* 2002;37:1-32.
18. Lewus RK, Carta G. Protein adsorption and transport in charged gels and chromatography media for protein separations. in Kaneko, K, Kanoh, H, Hanzawa, Y. Fundamentals of adsorption 7. Chiba, Japan: International Adsorption Society, IK International. 2002:117-124.
19. Ljunglöf A, Hjorth R. Confocal microscopy as a tool for studying protein adsorption to chromatography matrices. *J Chromatogr. A*. 1996;743:75-83.
20. Ljunglöf A, Thömmes J. Visualizing intraparticle protein transport in porous adsorbents by confocal microscopy. *J Chromatogr. A*. 1998; 813:387-395.
21. Linden T, Ljunglöf A, Kula MR, Thömmes J. Visualizing two component protein diffusion in porous adsorbents by confocal scanning laser microscopy. *Biotechnol Bioeng*. 1999;65:622-630.
22. Dziennik SR, Belcher EB, Barker GA, DeBergalis MJ, Fernandez SE, Lenhoff AM. Nondiffusive mechanisms enhance protein uptake rates in ion exchange particles. *Proc Natl Academ Sci*. 2003;100:420-425.
23. Hubbuch J, Linden T, Knieps E, Thömmes J, Kula M. Dynamics of protein uptake within adsorbent particles during packed bed chromatography. *Biotechnol Bioeng*. 2002;80:359-368.
24. Lewus RK, Carta G. Protein diffusion in charged polyacrylamide gels: visualization and analysis. *J Chromatogr. A*. 1999;865:155-168.
25. Lewus RK, Carta G. Protein transport in constrained anionic hydrogels: diffusion and boundary layer mass transfer. *Ind Eng Chem Research*. 2001;40:1548-1558.
26. Brooks CA, Cramer SM. Steric mass action ion-exchange - displacement profiles and induced salt gradients. *AIChE J*. 1992;38:1969-1978.
27. Gadam SD, Jayaraman G, Cramer SM. Characterization of nonlinear adsorption properties of dextran-based polyelectrolyte displacers in ion-exchange systems. *J Chromatogr. A*. 1993;630:37-52.
28. Iyer H, Tapper S, Lester P, Wolk B, van Reis R. Use of the steric mass action model in ion-exchange chromatographic process development. *J Chromatogr. A*. 1999;832:1-9.
29. Hunter AK, Carta G. Protein adsorption on novel acrylamido-based polymeric ion-exchangers, i. morphology and equilibrium adsorption. *J Chromatogr. A*. 2000;897:65-80.
30. Schmidt B, Wandrey C, Freitag R. Investigation of particle-based and monolithic columns for cation exchange protein displacement chromatography using poly(diallyl-dimethylammonium chloride) as displacer. *J Chromatogr. A*. 2003;1018:155-167.

Manuscript received June 16, 2004, and revision received Dec. 10, 2004.